Sedimentary and geochemical evidence of Eocene climate change in the Xining Basin, northeastern Tibetan Plateau

Abu Sadat Md SAYEM[1,2,3], Zhengtang GUO[1,2,4*], Haibin WU[1,2], Chunxia ZHANG[1,4], Fan YANG[1,2], Guoqiao XIAO[5] & Zhilin HE[1,2]

[1] *Key Laboratory of Cenozoic Geology and Environment, Institute of Geology and Geophysics, Chinese Academy of Sciences, Beijing 100029, China;*
[2] *University of Chinese Academy of Sciences, Beijing 100049, China;*
[3] *Department of Geological Sciences, Jahangirnagar University, Dhaka 1342, Bangladesh;*
[4] *CAS Center for Excellence in Life and Paleoenvironment, Beijing 100044, China;*
[5] *State Key Laboratory of Biogeology and Environmental Geology, School of Earth Sciences, China University of Geosciences, Wuhan 430074, China*

Abstract   The northeastern Tibetan Plateau began to grow during the Eocene and it is important to understand the climatic history of Asia during this period of so-called 'doubthouse' conditions. However, despite major advances in the last few decades, the evolutionary history and possible mechanisms of Eocene climate change in the northeastern Tibetan Plateau remain unclear. The Xining Basin in the northeastern Tibetan Plateau contains a continuous sequence of Early to Late Eocene non-marine sediments which provides the opportunity to resolve long-term climate changes during this period. In this study, we report the results of analyses of lithofacies, sediment color and geochemistry of bulk samples collected from the Xijigou section of the Xining Basin. An abrupt lithofacies change between the Early (~52–40 Ma) and Late Eocene (~40–34 Ma) indicates a change in the depositional environment from a shallow lake to a playa lake in response to a significant climatic shift. During ~52–40 Ma, higher values of sediment redness (a^*), redness/lightness (a^*/L^*) and higher modified Chemical Index of Weathering (CIW′) indicate a relatively warm and humid climate, while from ~40–34 Ma the lower values of a^*, a^*/L^* and lower CIW′ imply sub-humid to semi-arid climatic conditions. The paleoclimatic records indicate a long-term (~52–34 Ma) trend of decreasing chemical weathering, consistent with global climate change. An abrupt sharp excursion of the proxy records during ~42–40 Ma suggests a relatively brief warm interval, corresponding to the Middle Eocene Climatic Optimum (MECO). We suggest that global cooling substantially reduced humidity in inner Asia, resulting in sub-humid to semi-arid climatic conditions after 40 Ma in the Xining Basin, which may have been responsible for the long-term trend of decreasing chemical weathering during the Eocene.

Keywords   Eocene, Climate change, Sediment color, Chemical index of weathering, Xining Basin, Tibetan Plateau

1. Introduction

During the Cenozoic there was a major change in global climate from 'greenhouse' conditions during the Paleocene-Early Eocene to 'icehouse' conditions during the Oligocene (Zachos et al., 2001; Bohaty and Zachos, 2003). The depletion of atmospheric CO_2 together with the growth of Antarctic ice sheets are considered to be the driving me-

---

* Corresponding author (email: ztguo@mail.iggcas.ac.cn)

chanisms of global climate change during the Eocene (Pagani et al., 2005; Zachos et al., 2008; Pearson et al., 2009; Anagnostou et al., 2016). However, the magnitude of the influence of these global factors on Asian climate change during the Eocene is still debated (Dupont-Nivet et al., 2007; Abels et al., 2011; Song et al., 2013; Zhang and Guo, 2014; Fang et al., 2015; Tada et al., 2016).

The present-day northeastern Tibetan Plateau is located in an inland arid region. The climate of the region evolved from a 'planetary' subtropical arid zonal pattern in the Paleogene to a monsoon-dominated 'inland' arid pattern by the early Miocene (Guo et al., 2008). Despite several decades of research, there is a still controversy regarding the climatic evolution of central Asia during the Eocene. Various lines of evidence from the sedimentary basins of the Tibetan Plateau suggest that the climate changed from warm and humid to cold and dry in the Late Eocene and that aridification in the Asian interior commenced before and/or during the Eocene-Oligocene transition (EOT) (Dupont-Nivet et al., 2007; Hong et al., 2010; Xiao et al., 2010; Long et al., 2011; Hoorn et al., 2012; Song et al., 2013; Zhang and Guo, 2014). Rock magnetics and *n*-alkane records from the northeastern Tibetan Plateau show a long-term cooling trend from the Early Eocene to the Early Miocene (Long et al., 2011; Fang et al., 2015). However, a recent climate simulation indicated that a monsoon-like climate occurred in the northeastern Tibetan Plateau since the late Eocene (Licht et al, 2014). Previous studies have shown that Eocene climate change in central Asia was closely associated with Tibetan Plateau uplift, retreat of the Parathethys Sea and global cooling (Dupont-Nivet et al., 2007; Zhang et al., 2007; Abels et al., 2011; Bosboom et al., 2011, 2014; Hoorn et al., 2012; Tada et al., 2016). However, the relationship and linkage of these driving factors to Eocene climatic variability in the Asian interior remains unclear. In addition, the consistency or otherwise of Eocene climatic responses in inner Asia with marine records is poorly documented. Therefore, new proxy data from the Tibetan Plateau basins and their comparison with marine records are needed to unravel the Eocene climate history in central Asia.

The Eocene is regarded as a 'doubthouse' in terms of global climate conditions, given the climatic deterioration from a Paleocene-Early Eocene 'greenhouse' state to an Oligocene 'icehouse' state (Zachos et al., 1996; Miller et al., 2005). Until now, most of the available Eocene paleoclimatic records are from marine sediments which recorded maximum temperatures in the Early Eocene, followed by a general cooling trend towards the EOT and accompanied by short-duration warming events (Zachos et al., 2001, 2008; Bohaty and Zachos, 2003). However, compared with marine records, the nature of continental climate change during the Eocene, especially in central Asia, is little known. Recently, various proxy records from the Tibetan Plateau have been considered, but most are limited either to the EOT (Dupont-Nivet et al., 2007; Xiao et al., 2010; Bosboom et al., 2011, 2014; Zhang and Guo, 2014) or the Late Eocene (Abels et al., 2011; Long et al., 2011; Hoorn et al., 2012; Licht et al., 2014) and there is a substantial controversy regarding the interpretation of Eocene climate change. Furthermore, paleoclimatic studies of the Early Eocene are sparse. Therefore, more terrestrial climatic records with reliable proxies are needed to clarify the nature of Asian climate changes during the Eocene.

The Xining Basin in the northeastern Tibetan Plateau contains long and continuous sequence of Eocene sediments (Dai et al., 2006; Xiao et al., 2012) and thus is highly suited to clarify the paleoclimatic history of the region during the Eocene. Most importantly, the Xining Basin is located in the area where the impacts of Tibetan Plateau uplift, origin of the Asian monsoon and global temperature changes are all preserved within the sedimentary strata. Biostratigraphic and magnetostratigraphic studies have confirmed the age of the Xining Basin sediments (Li and Qiu, 1980; Qiu and Qiu, 1995; Horton et al., 2004; Dai et al., 2006; Xiao et al., 2012) and Abels et al. (2011) and Zhang et al. (2016) have outlined the results of paleoenvironmental studies of the Eocene strata. Here, we present the results of detailed analyses of lithofacies, sediment color and geochemical proxies of Eocene strata from the Xining Basin which are used to try to unravel the Eocene paleoclimatic history in the northeastern Tibetan Plateau. The well-exposed and continuous Eocene sedimentary sequence of the Xijigou section (XG) was selected (Figure 1). Our records are correlated with other regional paleoclimatic records and with the marine δ^{18}O record and the findings are used to interpret Eocene climatic history and specifically to discuss possible driving mechanisms.

2. Geological setting

The Xining Basin is a part of the Paleocene-Miocene Basin system located in the northeastern margin of the Tibetan Plateau (Figure 1). Its formation is related to Late Jurassic-Early Cretaceous extension followed by Early Cretaceous-Paleogene regional post-rift thermal subsidence (Dupont-Nivet et al., 2004; Horton et al., 2004). It is a sub-basin of the greater Longzhong Basin and covers an area of about 7400 km^2. Locally, the Xining Basin is limited to the Daban Shan to the north, the Laji Shan to the south and the Riyue Shan to the west (Figure 1); to the east a small uplifted area separats the Xining Basin from the Lanzhou Basin. Tectonically, the Xining Basin is bordered by the transpressional Middle Qilian Shan Fault system in the north and the Laji Shan Fault system of the same nature to the south (Figure 1). The structural trends vary substantially between the southern and northern parts of the basin. In the south, the Cenozoic
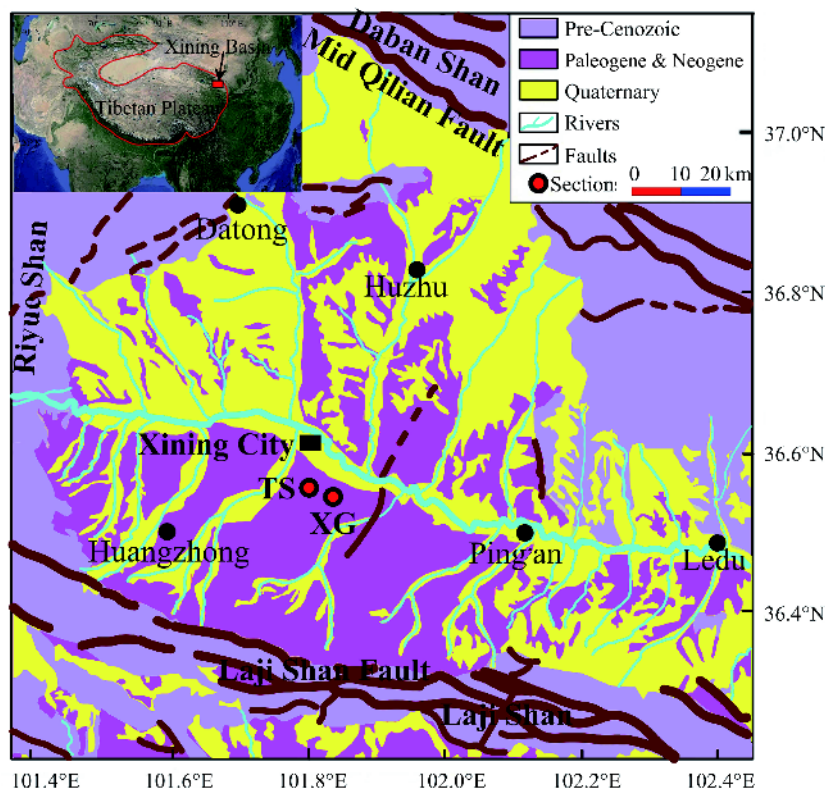
Figure 1 Geologic map of the Xining Basin (slightly modified after Xiao et al., 2012) showing the location of the Xijigou section (XG) and Tashan section (TS).

sequences are characterized by NNE-SSW trending structures, whereas in the north the basin is characterized by E-W trending structures. The present-day elevation of the basin ranges between ~2100 and ~3000 m above mean sea level (MSL). Modern annual mean temperature (~6°C) and precipitation (~478 mm) suggest that the Xining Basin is dominated by an arid/semiarid continental climate and is influenced by the East Asia summer monsoon.

The base of the Cenozoic stratigraphy of the Xining Basin is unconformable on the Late Cretaceous basement (QBGMR, 1985, 1991; Dai et al., 2006). Previous studies revealed Early Eocene (~52 Ma) to Early Miocene (~16 Ma) continuous sedimentation with a thickness of more than 800 m (QBGMR, 1985, 1991; Dai et al., 2006; Xiao et al., 2012). The stratigraphic successions of the basin can be divided into two groups: the Paleogene Xining Group and the Neogene Guide Group. The magnetostratigraphy of the well-exposed Xiejia section (Dai et al., 2006) and Tashan section (Xiao et al., 2012) confirmed the age of the strata in the Xining Basin from ~52 Ma to ~16 Ma. The lower Xining Group consists of the coarse-grained sandy Qijiachuan Formation (>52 Ma), reddish muddy Honggou Formation (52–41.5 Ma) and the cyclically-alternating red mudstone and gypsiferous Mahalagou Formation (41.5–25 Ma) (Figure 2a). The upper Guide Group contains the reddish-brown muddy Xiejia Formation (25–23 Ma), the yellowish-brown

muddy Chetougou Formation (23–18 Ma) and the pale yellowish silty Xianshuihe Formation (18–16 Ma) (Figure 2a).

In this study, we focus on Eocene (52–34 Ma) continental records from the Xining Basin which comprise the Honggou Formation and the Lower and Middle Mahalagou Formation. The sedimentary evidence indicates that the paleoenvironment of the Honggou Formation was lacustrine, whereas that of the Lower and Middle Mahalagou Formation was a playa lake environment (Dai et al., 2006; Dupont-Nivet et al., 2007; Abels et al., 2011; Zhang et al., 2016). Pollen records from the Xining Basin indicate that warm-temperate xerophytic taxa (*Ephedra* and *Nitraria*) dominated the Honggou Formation and cool-preferring conifers (*Picea* and *Pinecea*) prevailed within the Mahalagou Formation (Dupont-Nivet et al., 2008; Long et al., 2011). To characterize Eocene climatic variability, we collected continuous bulk samples from the Xijigou section (XG; 101°52′E, 36°31′N), located in the mid-southern part of the Xining Basin, ~14 km south of Xining City (Figure 1).

3. Material and methods

The Eocene stratigraphic interval measured in the Xijigou section is 278 m thick. An additional 26 m of the middle Mahalagou Formation from the Tashan section, ~4 km west
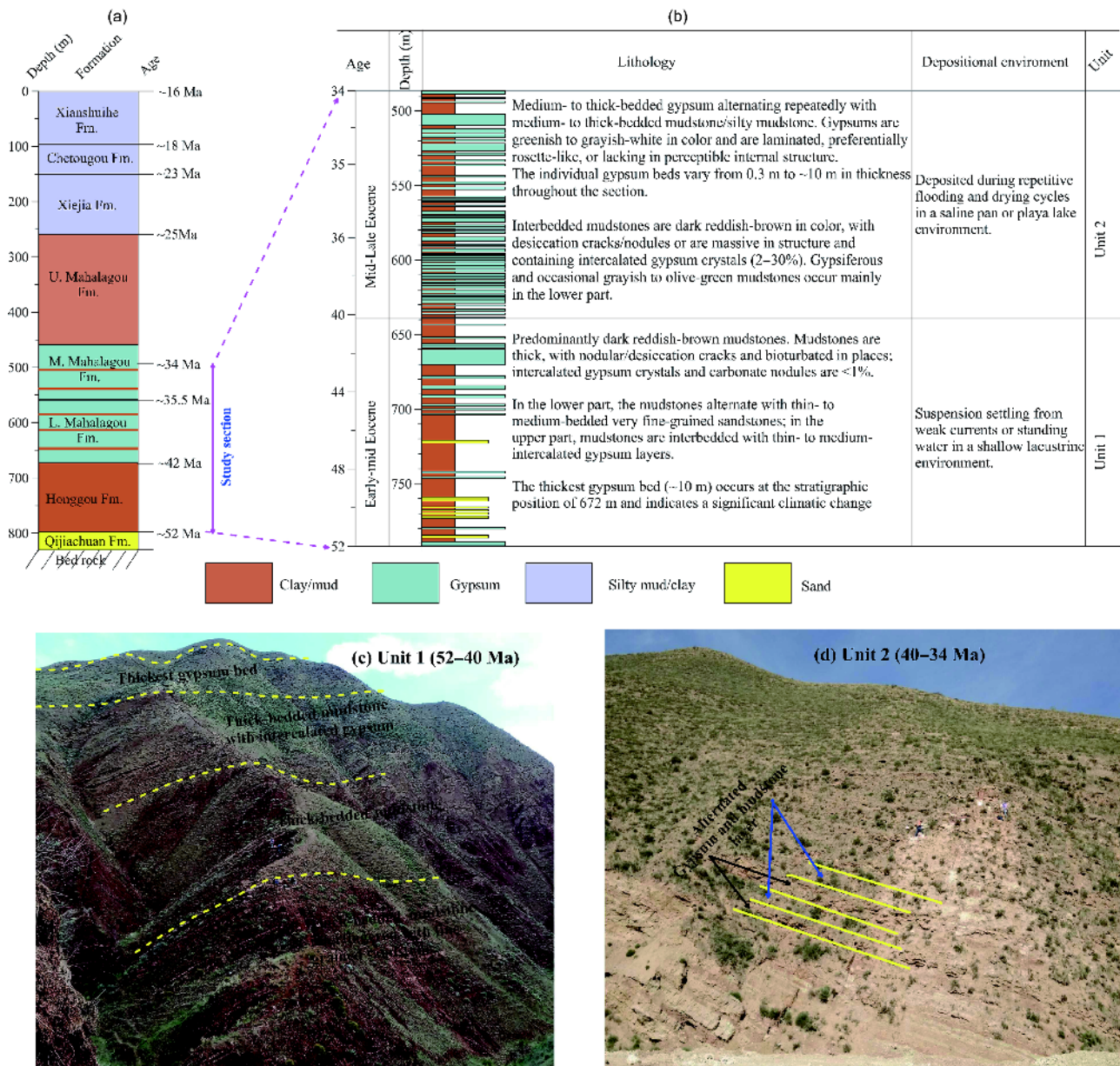
Figure 2   (a) Generalized Cenozoic stratigraphy of the Xining Basin (modified and continued after Xiao et al., 2012). (b) Detailed vertical lithostratigraphy and lithology of the Eocene sediments from the Xijigou section and Tashan section (lower 26 m) of the Xining Basin (formation ages are adopted from Dai et al., 2006 and Xiao et al., 2012). (c) Outcrop view of Unit 1 (~52–40 Ma) displaying the dominance of dark reddish-brown mudstone lithofacies; the thickest gypsum bed (~10 m) at the top represents a significant depositional and climatic shift. (d) Outcrop view of Unit 2 (~40–34 Ma) showing the dominance of alternating gypsum and mudstone lithofacies.

of the Xijigou section (Figure 1), was included to complete the Eocene sedimentary profile. For stratigraphic correlation between the two sections, the gypsum beds were carefully examined following Xiao et al. (2010) and bed-to-bed correlation was performed. The gypsum beds of the Xijigou section were found to correlate well with those of the Tashan section (Appendix Figure S1, http://earth.scichina.com). Gypsum bed G_4, which represents the Eocene-Oligocene Boundary (EOB) in the Tashan section (~33.8 Ma; Xiao et al., 2010), correlates well with G_0 (34 Ma) in the Xiejia section (Dupont-Nivet et al., 2007) (Appendix Figure S1a–

c); it also correlates to the same polarity chron, C13r, in both sections. Therefore, the top of the Eocene profile in this study is taken as ~34 Ma in age. In addition, the magnetostratigraphic ages of Xiao et al. (2010, 2012) are widely accepted because of the high-resolution record and so, we adopted their age model for the depth interval upto 560 m. Since, no new magnetostratigraphic data are available for the Honggou Formation and Qijiachuan Formation, we adopted the interpretation of Dai et al. (2006) for stratigraphic correlation in the lower part of the Xijigou section (Appendix Figure S1c and d). To further constrain the ages of the Eo-

cene strata in the Xining Basin we also collected samples for a high-resolution magnetostratigraphic study of the Xijigou section which is in progress and will be published elsewhere.

For the present study, bulk samples were collected from the Xijigou section and air-dried at room temperature prior to laboratory analyses. All the laboratory work was performed in the State Key Laboratory of Cenozoic Geology and Environment, Institute of Geology and Geophysics, Chinese Academy of Sciences.

Color is a fundamental sedimentary property depends on the mineral composition and organic matter content of the sediments. After deposition it changes rapidly in a dry, oxidizing environment and hence reflects hot-warm and cold-dry climatic conditions (Nagao and Nakashima, 1992). In this study, the color parameters L^*, a^* and b^* (CIE, 1978) are used to characterized color variability of the Eocene sediments from the Xining Basin for paleoclimatic reconstruction. The samples were ground to powder and placed in plastic boxes after weighing. Color reflectance was measured using a Konica Minolta CM–700d colorimeter at a 3 m stratigraphic interval. Chromaticity L^* reflects lightness and higher values indicate a cold and dry climate. The degree of redness (a^*) reflects the content of fine-grained hematite (Nie et al., 2010) and largely indicates the soil/sediment temperature (Guo et al., 1998, 2009; Yang and Ding, 2003; Torrent et al., 2006, 2010; Gao et al., 2018). There is controversy regarding the interpretation of soil/sediment reddening (Maher, 1998; Torrent et al., 2006, 2010); however, Gao et al. (2018) proposed a novel interpretation of hematite formation in the natural environment, which suggested that high ambient temperatures favored hematite formation during weathering processes through the transformation of maghemite to hematite, as well as directly from ferrihydrite to hematite. In addition, it has been demonstrated that the concentration of hematite increases despite decreasing dryness (Gao et al., 2018). Therefore, the formation of fine-grained hematite during weathering is primarily dependent on temperature, which provides a basis for paleoclimatic reconstruction with higher values of a^* corresponding to a warmer climate. Chromaticity b^* indicates the degree of yellowness, with higher values reflecting increased effective moisture and vice versa (Wu and Li, 2004).

Variations of major and minor elemental ratios are often used as paleoclimatic proxy for soil and lake sediments (Lo et al., 2017). In this study, major element geochemistry of the Eocene bulk samples from the Xining Basin (at a 3-m spacing) was used for paleoclimatic reconstruction. The degree of weathering intensity is estimated using the modified Chemical Index of weathering (CIW′) and various ratios (molecular ratio) of the major and minor elements. CIW′ is calculated as $[Al_2O_3/(Al_2O_3+Na_2O)] \times 100$. Here, CIW′ is used as a proxy instead of the Chemical Index of Alteration (CIA) and Chemical Index of Weathering (CIW), because our samples contained relatively high percentages of CaO (average >19%); in this case the use of CIA and CIW could result in the misinterpretation of chemical weathering (Cullers, 2000). The analysis was performed by X-Ray fluorescence (XRF) using a PANAnalytical spectrometer. About 5 gm of each sample were measured and ground to a powder in an agate mortar. All the samples were treated with 10% H_2O_2 and 1% CH_3COOH to remove organic matter and carbonates, respectively. After drying, fused pellets were prepared using a mixture of 0.7 g of powdered sample and 7 g of lithium tetraborate at a temperature of 1100°C. About 100 g of each sample were heated at 1000°C to measure the weight loss on ignition (LOI) prior to the treatment.

4. Results

4.1 Sedimentary lithofacies

The Eocene sedimentary sequence of the Xining Basin exhibits a distinct pattern of lithofacies variation and is divided into two units (Figure 2b): Unit 1 (from 794–640 m depth) and Unit 2 (from 640–490 m depth). Previous magnetostratigraphic studies (Dai et al., 2006; Xiao et al., 2012) indicate ages ranges of ~52–40 Ma and ~40–34 Ma for Units 1 and 2, respectively. The lithology and lithofacies of the units are described below.

Unit 1 is 154 m thick and predominantly composed of thick, dark reddish-brown mudstone (Figure 2c). The mudstones are massive, with nodular/desiccation cracks and a laminated structure and are bioturbated in places. Intercalated gypsum crystals and carbonate nodules are present in minor amounts (<1%). The lithofacies vary within the lower, middle and upper part of the unit. In the lower part, mudstones are intercalated with thin-to medium-bedded, very fine-grained sandstone and occasional gypsum layers, whereas thick-bedded mudstones are dominant in the middle part (Figure 2b). Conversely, in the upper part, mudstones are intercalated with gypsum layers on a centimeter scale. The thickest gypsum bed (~10 m) within the entire Eocene profile occurs at the stratigraphic position of ~670 m (Figure 2b). The thick and dark reddish-brown mudstones are interpreted as being deposited from suspension in weak currents or in standing water in a shallow lacustrine environment. The dark reddish-brown color is due to the high degree of oxidation. Nodular and desiccation crack structures indicate sediment compaction and drying after deposition respectively. The presence of carbonate nodules and evidence of biological activity imply a lacustrine environment and relatively warm climatic conditions. The occurrence of the thickest gypsum bed represents a transition of the depositional environment due to a significant climatic shift in the Middle Eocene.

Unit 2 is 150-m thick and consists of medium- to thick-

bedded gypsum layers repeatedly alternating with medium- to thick-bedded mudstone/silty mudstone (Figure 2b and d). The gypsums are greenish to grayish-white in color and are laminated and preferentially rosette-like or they lack a perceptible internal structure. The individual gypsum beds vary from 0.3 to ~10 m in thickness throughout the section. Overall, the interbedded mudstones are dark reddish-brown in color, with desiccation cracks/nodules or are massive in structure and contain intercalated layers of gypsum crystals (2–30%). Gypsiferous and occasional grayish to olive-green mudstones occur mainly in the lower part of Unit 2. The abundance of the gypsum beds alternates with mudstones indicating repeated wet and dry cycles in a saline pan/playa lake environment. The variations of lithofacies color suggest alternating oxidizing and reducing conditions.

4.2 Changes in sediment color

The vertical distributions of the sediment color reflectance parameters are illustrated in Figure 3. The average values of lightness (L^*), redness (a^*) and yellowness (b^*) across the Eocene sedimentary sequence in the Xining Basin are 68.90, 15.60 and 5.54, respectively. The values of lightness, redness and yellowness of the natural samples correspond well with the alternating mudstone and gypsum layers. The gypsum layers correspond to intervals of low redness and yellowness values and high lightness values, whereas the mudstone layers correspond to high redness and yellowness values and low lightness values (Figure 3). All the sediment color indices exhibit marked variations from 52–40 Ma (Unit 1) and from 40–34 Ma (Unit 2).

The redness values (avg. 6.01) and yellowness values (avg. 16.62) are higher from 52–40 Ma than from 40–34 Ma (avg. 4.99 and 14.57, respectively). In contrast, the average lightness value is lower during 52–40 Ma (68.00) than during 40–34 Ma (69.79). This indicates that the Early-mid Eocene sediments were deposited under warmer and more humid conditions than those of the mid-Late Eocene. During 52–40 Ma, maximum values of redness and yellowness and minimum value of lightness are evident below 740 m, where the parameters fluctuate significantly due to the occurrence of intercalated gypsum layers. Above 740 m, the upwards decreases in redness and yellowness and increasing lightness trends are interrupted by a sharp excursion from 670–640 m (~42–40 Ma; Figure 3). During 40–34 Ma, the sediments are characterized by repeated brief fluctuations in redness, lightness and yellowness, together with alternating mudstone and gypsum layers (Figure 3), which suggest periodic oscillations of humid-to-dry and warm to-cool climatic conditions.
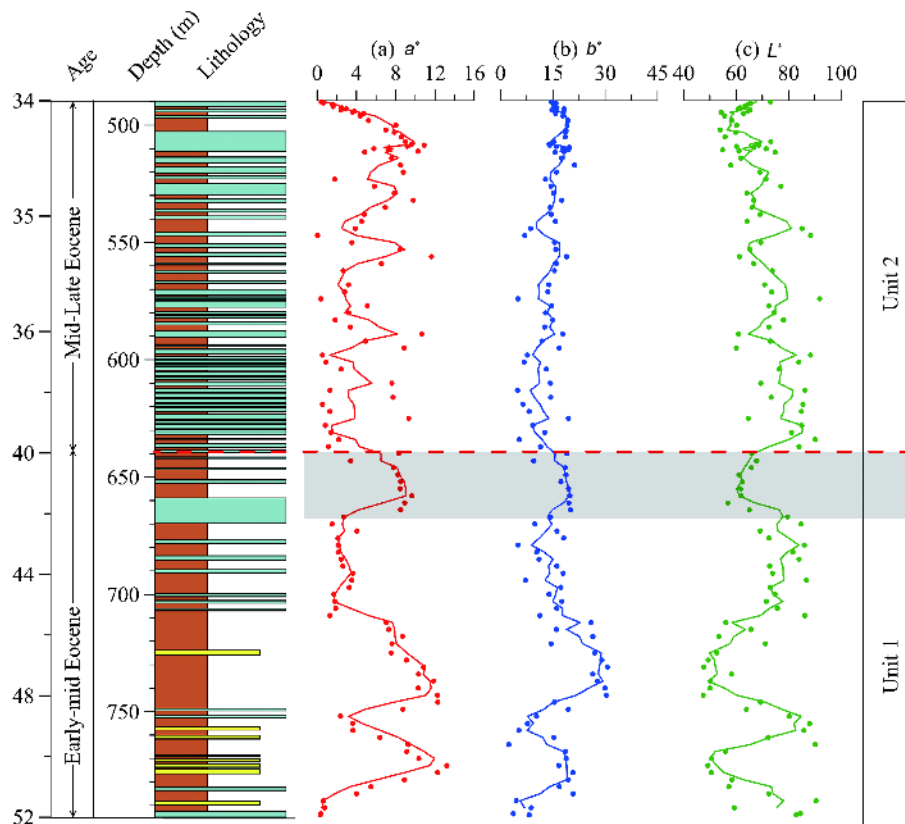

Figure 3 Vertical distribution of sediment color parameters of the Eocene sediments of the Xining Basin: (a) redness (a^*); (b) blueness (b^*); (c) yellowness (L^*). Shaded area indicates an abrupt excursion of the proxies.

4.3 Changes in geochemical properties

The Eocene bulk sediments from the Xining Basin are characterized by high concentrations of SiO_2, SO_3, CaO, Al_2O_3 and low concentrations of Fe_2O_3, K_2O, Na_2O, MgO, TiO_2, MnO and P_2O_5 (Appendix Table A1). The concentration of SiO_2 varies substantially within the studied section, ranging from 0.06% to 66.94% (avg. 25.69%). The SO_3 concentration ranges between 0% and 50.50% (avg. 25.84%). The samples show marked variations in CaO and Al_2O_3 concentration, ranging from 0.14% to 35.83% (avg. 19.54%) and from 0.25% to 19.99% (avg. 7.88%), respectively. The other major oxides, Fe_2O_3, K_2O, Na_2O, MgO, TiO_2, MnO and P_2O_5, do not vary significantly (Subsequently, the major oxides are labeled Fe, K, Na, etc.).

The linear relationships of the major elements with respect to Al_2O_3 are displayed in Figure 4, where plots of UCC data (Taylor and McLennan, 1985) are used for reference. The positive correlation of SiO_2 with Al_2O_3 (Figure 4a) throughout the Eocene sequence implies silica-rich material affiliated with Al-rich clay- and silt-sized particles. The moderate to strong positive affinity of Al_2O_3 with Fe_2O_3, K_2O, MnO and TiO_2 (Figure 4b, d, g and h) suggests that the enrichment of Fe, K, Mn and Ti is associated with phyllosilicates, especially illite (Dabard, 1990). The relationships of Na_2O and MgO with Al_2O_3 exhibit a moderate positive correlation (Figure 4c and e) indicating that the enrichment Na and Mg is related to a chlorite matrix (Dabard, 1990). In all the bi-plots referenced above, the sediments of Unit 2 show stronger positive correlations and a wider range of values than those of Unit 1, suggesting that the sediments from 40–34 Ma contain more illite and chlorite in comparison with those from 52–40 Ma. CaO is negatively correlated with Al_2O_3 (Figure 4f), where the sediments from 52–40 Ma exhibit larger values, suggesting a reduction in more labile Ca^{2+} from calcite and feldspar during intense chemical weathering. The relationship of Al_2O_3 and P_2O_5 (Figure 4i) is weak and no obvious relation exists in the bi-plot diagram. Overall, all the bi-plots for the major elements of the Eocene sediments exhibit good linear correlations (Figure 4).

The elemental (molecular) ratios of Na/Al, Na/Ti, K/Na, CIW′ and binary plot of K vs. Rb were used to characterize variations in weathering intensity in the source area. Under hot and humid conditions, intense chemical weathering results in the preferential leaching of more mobile elements like Na, K and Ca compared to more stable elements like Al, Ti or Rb, and vice versa (White et al., 1999). The elemental ratios of Na/Al and Na/Ti decrease due to the rapid loss of Na or the enrichment of Al or Ti, and the K/Na ratio decreases because K is more stable than Na during weathering (Nesbitt et al., 1996). A plot of K vs. Rb can be used to indicate levels of weathering in the source area since K is more labile relative to Rb (Nesbitt et al., 1980). The degree of chemical weathering is obtained by employing the modified form of the Chemical Index of Weathering (CIW′; Cullers, 2000), with lower values indicating weaker chemical weathering within the weathering profile.

The vertical distributions of the elemental ratios and CIW′ of the Eocene sediments from the Xining Basin are illustrated in Figure 5. There are distinct differences between Unit 1 (52–40 Ma) and Unit 2 (40–34 Ma) which are consistent with lithofacies variations and sediment color characteristics (Figure 3). Unit 1 is characterized by lower values of Na/Al (avg. 0.14) and Na/Ti (avg. 6.74) and higher value of K/Na (avg. 2.51) compare to Unit 2 (in which the respective average values are 0.20, 10.36 and 1.34). The CIW′ values of Unit 1 range from 78.37–97.77 (avg. 87.58), whereas in Unit 2 the values range from 72.92–92.82 (avg. 83.96). Therefore, all these weathering indicators indicate moderate to intense chemical weathering during 52–40 Ma and moderate chemical weathering during 40–34 Ma in the source region. The vertical trends of Na/Al and Na/Ti in Unit 1 are similar with lowest values around 51–50 Ma, followed by an upwards increasing trend which is interrupted by an abrupt decrease from 670–640 m (~42–40 Ma; Figure 5a and b). Above 640 m, the values of the proxies decrease upwards with rhythmic minor fluctuations and a prominent brief increase at 510 m (~34.2 Ma). In contrast, K/Na and CIW′ exhibit maximum values around 51–50 Ma with a decreasing upwards trend and an abrupt positive excursion at 670–640 and 510 m (Figure 5c and d). Overall, the long-term upwards increasing trends of Na/Al and Na/Ti and upwards decreasing trends of K/Na and CIW′ indicate the weakening of chemical weathering from the Early to the Late Eocene (~52–34 Ma) in the Xining Basin.

Previous studies (Ferrell and Brooks, 1971; Timperley and Vigor-Brown, 1985; Liu et al., 2011) suggested that water in playa lakes or continental shallow lacustrine basin is lost lakes only through evaporation because of their endorheic character, where the mass flows of major ions Na^+, K^+, Ca^{2+}, Mg^{2+}, SO_4^{2-}, Cl^- and HCO_3^- are more associated with the surface waters draining the lake catchment than with the mass flows of major ions leaving the lake and ions are incorporated within the sediments. In saline lakes or in a drying shallow lacustrine basin (evidenced from the desiccation cracks in the mudstone facies) the cations are dominated by Na^+, with some Ca^{2+} and Mg^{2+}, with the lowest content of K^+ (Liu et al., 2011). In addition, if the chlorinity of lake waters increases then the percentage of exchangeable Na increases (Ferrell and Brooks, 1971). In such types of sedimentary environments readily mobile elements like Na and their variation trends relative to immobile elements like Al, Ti, K indicates their relatively immobile properties during chemical weathering, consistent with those documented from weathering profiles and arid regions. The brief rhythmic short fluctuations of the proxy records in the Late Eocene
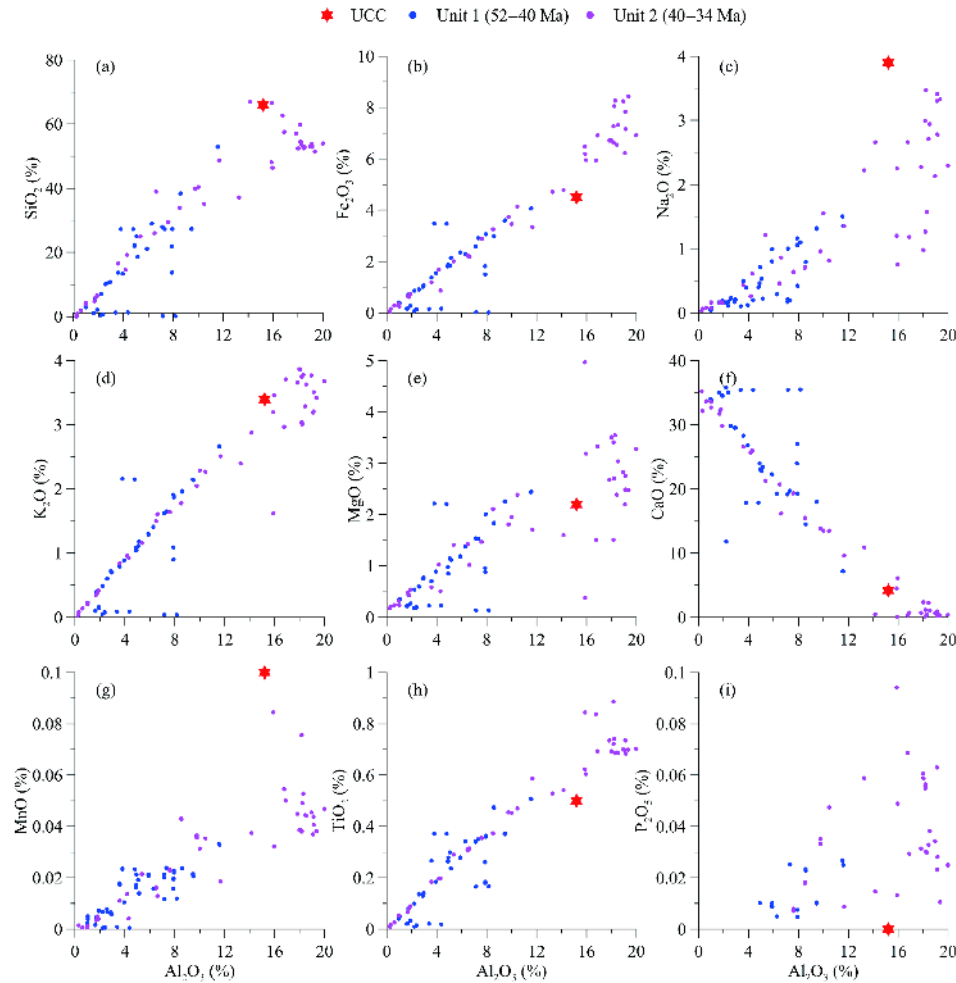
Figure 4   Bi-plots of major elements of the Eocene sediments for the Xining Basin. Blue and red dots represent samples from Unit 1 (52–40 Ma) and Unit 2 (40–34 Ma) respectively. UCC (Upper Continental Crust) data are adopted after Taylor and McLennan (1985).

(40–34 Ma), corresponding to alternating gypsum and mudstone layers, suggest rhythmic wet and dry oscillations.

The K/Rb ratios for the Eocene Xining Basin sediments (Figure 6) differ substantially from that of the upper continental crust (K/Rb=230) indicating moderate to intense chemical weathering in the source area. In addition, the samples from Unit 1 show a wider range of values and their distribution is distant from the K/Rb=230 line compared to Unit 2. This suggests stronger chemical weathering during 52–40 Ma compared to 40–34 Ma.

5.   Discussion

5.1   Eocene climates in the Xining Basin

The Eocene sedimentary sequence of the Xining Basin exhibits marked lithofacies differences (Figure 2b) between the Early (Unit 1, ~52–40 Ma) and Late Eocene (Unit 2, ~40–34 Ma). The thick-bedded red-mudstone-dominated (Figure 2c)

Early Eocene sediments were deposited in a shallow lacustrine environment; while the alternating gypsum layers and mudstones (Figure 2d) in the mid-Late Eocene suggest a saline/playa lake environment. There is no unconformity or interruption of deposition evident between the units. The occurrence of the thickest gypsum bed in the Middle Eocene (at the depth 670 m, ~42 Ma) and subsequent gypsum layers in the Late Eocene indicate the occurrence of significant climate change in the Xining Basin area; however, the linear positive correlations of the major elements (Figure 4) suggest that the provenance of the detritus did not change significantly during this period. This conclusion is in accord with that of previous studies (Duvall et al., 2011; Zhang et al., 2016) as well as with the constant low sedimentation rate (1.8 cm kyr^{-1}) throughout the Eocene in the Xining Basin (Dai et al., 2006).

Based on the abrupt lithofacies variations and the marked changes in sediment color and the variations of the major elements and weathering indices (Figures 2–6), two major
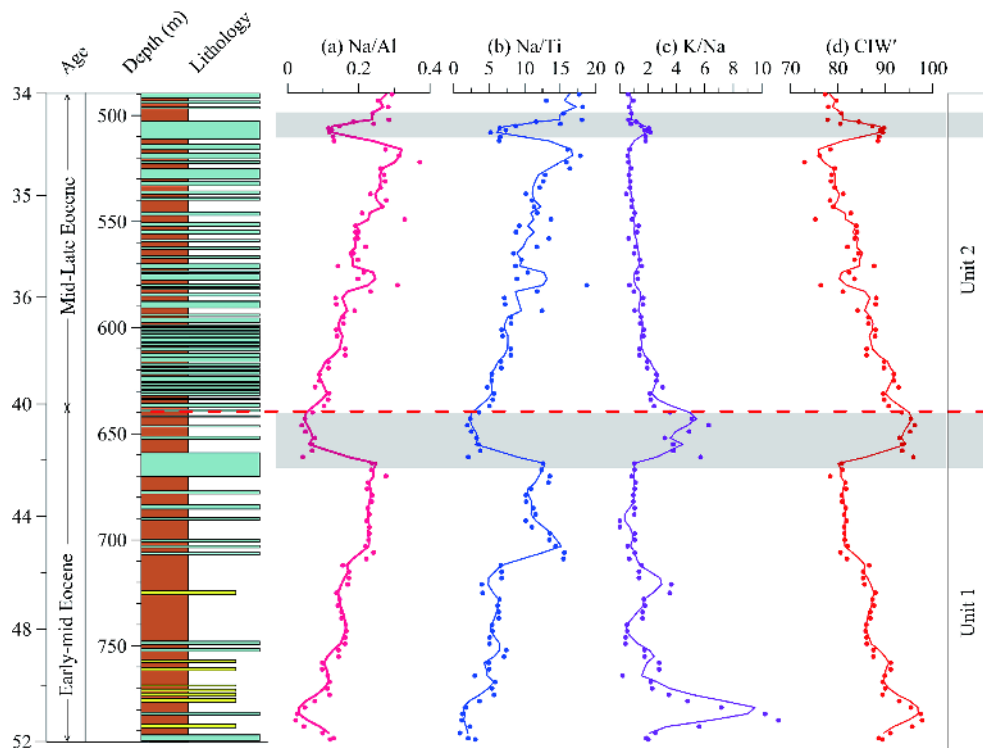
Figure 5   Vertical variations of Na/Al, Na/Ti, K/Na (molecular ratio) and Chemical Index of Weathering (CIW′) for the Eocene sediments of the Xining Basin.
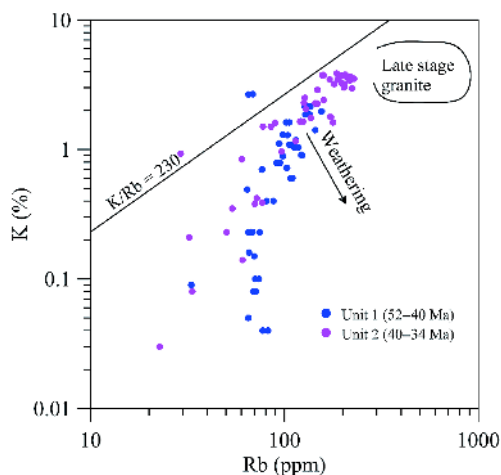

Figure 6   Plot of K vs. Rb (after Wronkiewicz and Condie, 1990) for the Eocene Xining Basin sediments. Blue dots and red dots represent the elemental (K/Rb) variation between Unit 1 (52–40 Ma) and Unit 2 (40–34 Ma), respectively. K/Rb=230 line indicates the average crustal ratio.

climatic episodes can be recognized across the Eocene sedimentary sequence of the Xining Basin (Figure 7). To obtain a better understanding of Eocene climate variability, our results were compared with coeval CIW′ records from the Qaidam Basin (Figure 7c; Song et al., 2013), pollen records from the Xining Basin (Figure 7d–h; Long et al., 2011) and with the deep marine $\delta^{18}O$ record (Figure 7i; Zachos et al., 2001, 2008).

5.1.1   Early-mid Eocene (~52 to 40 Ma) climatic change in the Xining Basin

Our results reveal an interval of climatic change from ~52 to 40 Ma (corresponding to Unit 1). As discussed above, the dark-reddish mud-dominated lithofacies, presence of carbonate nodules and evidence of biological activity indicate a shallow lacustrine environment under wet and warm conditions and a high degree of oxidation. During this interval (52–40 Ma), the sediments of the Xining Basin are characterized by lower average values of L^* (Figure 3c) and higher values of a^* and a^*/L^* ratio (Figures 3a and 7a), which indicate a warmer climate with a relatively high degree of oxidation. The higher average value of b^* (16.62) suggests moist conditions during this period. The higher average values of CIW′ (Figure 5d) and K/Rb (Figure 6) ratios indicate stronger chemical weathering during the Early-mid Eocene. Generally, higher temperature and precipitation promote stronger chemical weathering (White et al., 1999). During the weathering process magnetite is altered to maghemite and at higher degree of oxidation maghemite is transformed to hematite. Thus, the higher redness and a^*/L^* ratio in the Early Eocene sediments are linearly correlated with CIW′ (Figures 3c, 7a and 7b), which indicates that redness is an effective weathering proxy and implies a warmer climate. The lower average values of Na/Al, Na/Ti and higher K/Na ratio (Figure 5a–c) suggest the rapid loss of labile Na⁺ under intense chemical weathering. Therefore, all these lines of
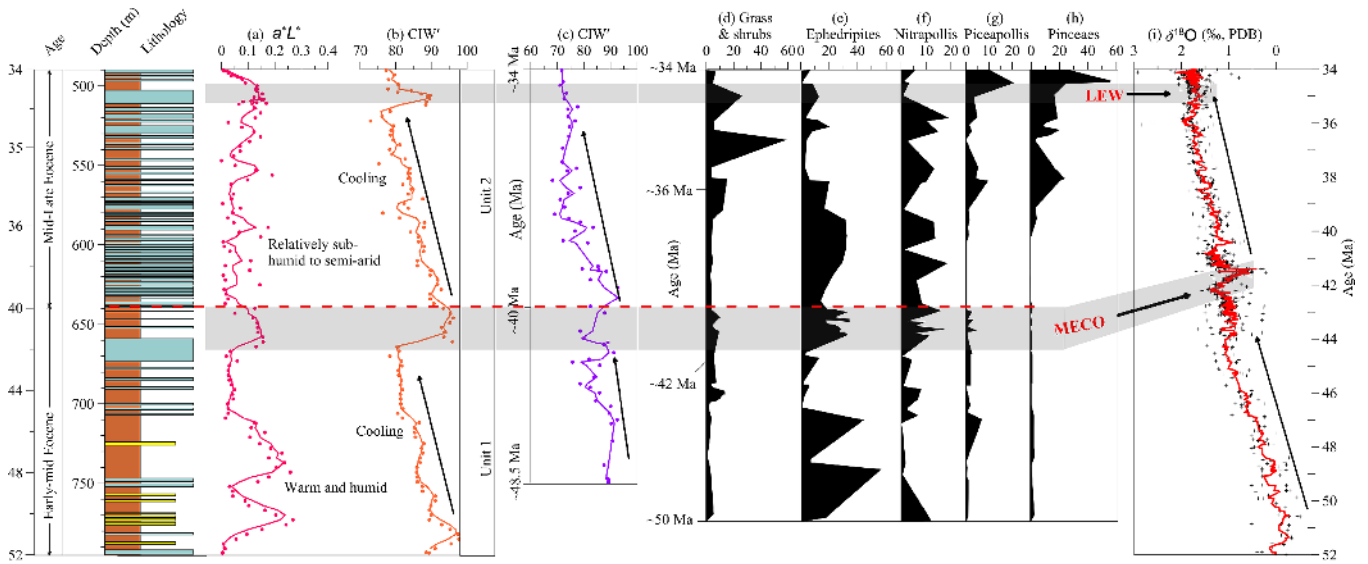
Figure 7   Comparison of the vertical variations of sediment color parameter a^*/L^* (redness/lightness, (a)) and Chemical Index of Weathering (CIW′, (b)) for the Eocene sedimentary sequence recorded in the Xining Basin. (c) Vertical variation of CIW′ from the Qaidam Basin (Song et al., 2013), northeastern Tibetan Plateau, on the same time scale. (d)–(h) Pollen diagram showing the abundance of major floral components (Long et al., 2011) recorded in the Xiejia section of the Xining Basin. (i) Variation of marine $\delta^{18}O$ records on the same timescale (Zachos et al., 2001). Shaded area indicates Eocene warming events, and MECO and LEW are the Middle Eocene Climate Optimum and Late Eocene Warming, respectively.

evidence strongly suggest the occurrence of a warm and humid climatic condition in the Xining Basin during the Early to Middle Eocene (~52–40 Ma).

This inference is also supported by the higher degree of chemical weathering (Figure 7c; Song et al., 2013) and lower chlorite content (Hong et al., 2010) recorded in the Early-mid Eocene sedimentary sequences of the neighboring Qaidam Basin in the northeastern Tibetan Plateau. Long et al. (2011) documented evidence for an environment with warm-temperate, sub-tropical deciduous xerophytic shrubs (*Ephedripites, Nitrapollis*) in the Early to Middle Eocene sediments of the Xiejia section of the Xining Basin (Figure 7d–f), whereas cool-preference conifers (*Piceapollis, Pinceaes*) were almost absent during this climatic interval (Figure 7g–h). Thus, it is very likely that warm and humid climatic conditions occurred around 52–40 Ma in the northeastern Tibetan region.

Maximum values of a^*/L^* ratio and CIW′ (Figure 7a and b) are evident at the beginning of the episode, followed by upwards-decreasing trends of these parameters which are interrupted by an abrupt positive excursion at around 42 Ma (Figure 7a–b). This implies that relatively moist condition and the maximum degree of chemical weathering and a warmer climate occurred in the Early Eocene which was succeeded by a trend of cooler and drier conditions until ~42 Ma. Thus, the upwards-decreasing trend of chemical weathering intensity was associated with a reduction in humidity from the Early to Middle Eocene. This decreasing trend of chemical weathering is in accord with global climatic cooling indicated by the marine $\delta^{18}O$ record (Figure 7i; Zachos et al., 2001). Clay mineral proxies from the Qaidam

Basin (Hong et al., 2010) and *n*-alkane records from the Xining Basin (Long et al., 2011) also support the occurrence of this cooling trend during the Early-mid Eocene in the northeastern Tibetan Plateau. Moreover, continental climatic records from Central Europe also revealed a similar cooling trend during 47.5–40 Ma (Mosbrugger et al., 2005).

The occurrence of the thickest gypsum bed (Figure 2b and c) and an abrupt increase in a^*/L^* and CIW′ ratios during ~42–40 Ma (Figure 7a and b) indicate a short-lived warming interval which agrees well with the sharp decrease in deep marine $\delta^{18}O$ at about 42 Ma (Figure 7i; Zachos et al., 2001). This short warming episode is termed the Middle Eocene Climatic Optimum (MECO; Bohaty and Zachos, 2003). The MECO event is recorded in the Qaidam Basin in the northeastern Tibetan Plateau (Figure 7c; Song et al., 2013), in the Fushan Basin in northeastern China (Quan et al., 2012), and in terrestrial records from western North America (Methner et al., 2016).

5.1.2   Mid-Late Eocene (~40 to 34 Ma) climatic change in the Xining Basin

The interval from ~40 to 34 Ma (Unit 2) is characterized by a marked change in sedimentary lithofacies (Figure 2b). The occurrence of thick gypsum layers alternating with mudstone layers suggests a significant change in the depositional environment due to a substantial climatic shift. The repetitive alternation of gypsum and mudstone facies (Figure 2d) indicates rhythmical wet and dry cycles in a playa lake setting under sub-humid/semi-arid climatic conditions. During this interval the sediments are characterized by higher average values of L^* and lower a^*/L^* ratios, which indicates a lower

degree of oxidation under sub-humid/semi-arid conditions in the Xining Basin. In Late Eocene (40–34 Ma), the vertical distribution of a^* and a^*/L^* values are characterized by slight upwards-increasing trends (Figures 3a and 7a). These contradictory trends are the result of abrupt lithological changes. The reflectance of redness and lightness fluctuated significantly during the period, corresponds well with the alternated mudstone and gypsum layers, which suggest periodic oscillation of warm to cold or wet to dry conditions. Although the entire Late Eocene period is characterized by alternating gypsum and mudstone beds, the vertical litholog of the Xijigou section (Figure 3) exhibits gypsum is the dominant lithofacies between 640 and 595 m depth. And above 595 m mudstone exceed the gypsum, can be formed more hematite during the warm period, which might be responsible for slight upwards-increasing trends of a^* and a^*/L^*. The lower average value of b^* (14.57) indicates a significant reduction in moisture content compared to the Early Eocene sediments.

The higher average values of Na/Al and Na/Ti and lower average values of K/Na, CIW′, K/Rb indicate weaker chemical weathering in the mid-Late Eocene. The linear relationships (Figure 4) and vertical distributions of the elemental ratios (Figure 5) indicate that the Late Eocene (40–34 Ma) sediments are enriched in Fe, Ti, Mn, Na and Mg compared to the Early Eocene (52–40 Ma), which suggests the enrichment of the clay minerals illite and chlorite during 40–34 Ma. Generally, illite and chlorite clay minerals form in cool and dry conditions (Chamley, 1989; Dabard, 1990). The vertical distributions of a^*/L^* ratio and CIW′ (Figure 7a and b) show a pattern of repeated minor fluctuations, which implies the alteration of wet and dry conditions. After the MECO, the long-term upwards-decreasing trend of CIW′ indicates weakening of chemical weathering in the Late Eocene (~40–34 Ma) due to a significant reduction in humidity. Thus, all the above lines of evidence imply a moderate degree of chemical weathering and warm-to-cold or wet-to-dry oscillations under sub-humid to semi-arid climatic condition in the Xining Basin during mid-Late Eocene time.

The foregoing interpretation is in accordance with the results of Long et al. (2011) who documented a reduction in the representation of the warm-temperate *Ephedripites* and *Nitrapollis* flora and the increasing representation of cool climate grasses, shrubs and conifers (*Piceapollis*, *Pinceaes*) (Figure 7d–h) within the Late Eocene sedimentary sequence in the Xining Basin. Furthermore, the lower index of chemical weathering (Song et al., 2013) and higher chlorite content (Hong et al., 2010) recorded in the Late Eocene in the Qaidam Basin also supports the occurrence of a cool and dry climate during this interval. Following the MECO, the long-term decreasing trend of chemical weathering until 34 Ma (Figure 7b) is in accord with the Late Eocene global cooling

recorded by the marine $\delta^{18}O$ record (Figure 7i). Palynological records from the Xining Basin (Dupont-Nivet et al., 2008; Long et al., 2011; Hoorn et al., 2012) and the nearby Qaidam Basin (Lu et al., 2010) indicate a trend of decreasing representation of higher and broad leaf plants and increasing representation of conifers, supporting the occurrence of a gradual cooling trend in the late Eocene. In addition, $\delta^{18}O$ records from lacustrine carbonates in the Qaidam Basin also document a gradual cooling trend from the Late Eocene to the Early Oligocene (Rieser et al., 2009).

In addition to the MECO, our paleoclimatic records reveal a very short and abrupt increase in the occurrence of warm and humid climatic fluctuations at ~34.2 Ma (Figures 5, 7a and 7b). Clay mineral records from the Tashan section of the Xining Basin also indicate similar warming oscillations at roughly the same time (Zhang and Guo, 2014). This warming event may correlate with the Late Eocene Warming (LEW) period which immediately preceded the Oligocene icehouse conditions (Bohaty and Zachos, 2003).

5.2 Driving mechanisms of Eocene climate change in the Xining Basin

The foregoing observations indicate that warm and humid climatic conditions in the Xining Basin occurred during the Early to Middle Eocene (~52–40 Ma), which changed progressively to sub-humid to semi-arid conditions in the mid–Late Eocene (~40–34 Ma). In addition, our results (Figure 7a and b) reveal a long-term trend of decreasing chemical weathering commencing at around 52 Ma and culminating at 34 Ma. The linkages and relative contribution of regional and global factors contributing to the observed Eocene climate variability in the Xining Basin are discussed below.

Although Tibetan Plateau uplift played an important role in influencing the Asian monsoon in the Early Miocene (Guo et al., 2002, 2008), it had little impact on Eocene climate change. In general, areas those are tectonically active and with high topographic are subjected to extensive erosion (Najman et al., 2008; Bracciali et al., 2015). The dominance of fine-grained lithofacies or absence of coarser particles and/or lack of an unconformity (Figure 2b–d) in the Xining Basin indicate that the northeastern Tibetan Plateau was not uplifted sufficiently to generate a corresponding sedimentary signal during this period. In addition, the low and constant sedimentation rate (1.8 cm kyr^{-1}) during 52–34 Ma (Dai et al., 2006) also supports this interpretation. Rather, the chemically precipitated gypsum layers during 40–34 Ma (Figure 2b, 2d) suggest that sedimentation in the Xining Basin was mainly controlled by climate rather than by tectonics at the time. In addition, tectonic forcing in a newly elevated area intensifies silicate weathering (Raymo and Ruddiman, 1992). The high concentration of SiO_2 (sandstones ~78–82%; mudrocks ~56–70%) in the Paleogene sediments from

the western Himalayan foreland basins indicates the extensive occurrence of silicate weathering in the uplifted Higher Himalaya (Singh, 2013), whereas the low concentration of SiO_2 (avg. ~25%) in the Eocene sediments of the Xining Basin suggests a lower degree of silicate weathering. This evidence confirms the relatively low relief of the Tibetan Plateau until the end of the period of concern. Furthermore, pollen records from the Lunpola Basin indicated that the paleo-altitude of Central Tibet was ~3000 m in the latest Oligocene-earliest Miocene (Sun and Jiang, 2013). All these lines of evidence argue against the view that the Tibetan Plateau was uplifted close to its present altitude before 40 Ma. Moreover, if the Tibetan Plateau had been uplifted to its present elevation at around 40 Ma, the Asian monsoon would have to have been established at that time (Guo et al., 2002, 2008). Conversely, our paleoclimatic records reveal sub-humid to semi-arid conditions and a general cooling trend throughout the Late Eocene (Figure 7b). Although palynological studies from the northeastern Tibetan Plateau sedimentary basins record the presence of taxa indicative of high-altitude vegetation at an optimal altitude of 1500–2500 m by the Late Eocene (Dupont-Nivet et al., 2008; Lu et al., 2010; Long et al., 2011; Hoorn et al., 2012), Tibetan Plateau uplift is not likely to have been the main factor responsible for the regional Eocene climatic conditions.

An additional regional factor, the retreat of the Paratethys Sea, can potentially explain the observed humidity changes in the Xining Basin during the Eocene. The humid climatic conditions in the Xining Basin around 52–40 Ma are consistent with the existence of the vast Paratethys Sea as the main source of moisture in Central Asia during the Paleogene-Early Eocene (Dercourt et al., 1993). The subsequent shrinkage of the Paratethys Sea due to global sea-level fall in the Late Eocene-Oligocene reduced humidity conditions in the Xining Basin area. Although the occurrence of a humid climate in the Early Eocene and reduction in humidity in the Late Eocene are consistent with the existence of a progressively shrinking Paratethys, it alone does not explain the long-term cooling trend in the Eocene (~52–34 Ma), and additional mechanisms, linked to global factors, must be responsible.

The factor responsible for the decreasing chemical weathering in the Xining Basin during the Eocene is likely linked to the global cooling recorded by the marine $\delta^{18}O$ record (Figure 7i). The growth of Antarctic ice-sheets commenced at ~43 Ma and expanded in the Oligocene (Zachos et al., 2001), while the Northern Hemisphere was ice-free until the Late Miocene (Lear et al., 2000). This global imbalance in the distribution of ice sheets would have resulted in a large latitudinal pressure contrast which forced the northward migration of subtropical highs in northwest China. This would have reduced humidity and promoted sub-humid to semi-arid climatic conditions across central Asia in the Late

Eocene. Thus, the reduction in humidity driven by Eocene global climatic cooling may be responsible for the long-term trend of decreasing chemical weathering in the Xining Basin. The northward migration of global climate zones would also have increased humidity conditions in South China (Guo et al., 2008), which would have periodically influenced the Xining Basin. These factors can potentially explain the short-duration cyclical humid and dry climatic oscillations in the Late Eocene (40–34 Ma). The sharp increases in the intensity of chemical weathering at around 42–40 Ma and 34 Ma may have been caused by a sudden increase in temperature and precipitation, which agrees well with the global marine oxygen isotope record.

6. Conclusions

We have used continuous sedimentary and geochemical data from the Xining Basin in the northeastern Tibetan Plateau to characterize regional climatic changes during the Early to Late Eocene (~52–34 Ma). During ~52–40 Ma, dark reddish-brown mudstone dominated the lithofacies indicating a shallow lacustrine environment with a high degree of oxidation. The occurrence of the thickest bed at ~42 Ma implies a marked change in depositional environment which we suggest was due to a significant climatic shift. The cyclic alternation of gypsum and mudstone lithofacies between 40 Ma and 34 Ma indicates that the sediments accumulated in a playa lake setting under oscillating wet/dry conditions. The lithofacies characteristics, relatively higher redness/lightness (a^*/L^*) ratio and stronger degree of chemical weathering indicate the occurrence of warm and humid climatic conditions in the Xining Basin during Early-mid Eocene time. The repetitive alterations of gypsum and mudstone facies, comparatively lower a^*/L^* ratios and weaker degree of chemical weathering with repetitive fluctuations indicate warm-to-cold or wet-to-dry oscillations under overall sub-humid to semi-arid climatic conditions during the mid-Late Eocene. The Chemical Index of Weathering (CIW′) record exhibits a long-term trend of decreasing chemical weathering from ~50 to 34 Ma, which may result from a reduction in humidity in the Xining Basin area. The trend of decreasing chemical weathering in the Xining Basin is in good agreement with the marine $\delta^{18}O$ record and both reflect global-scale Eocene climate change. The short-term Middle Eocene Climatic Optimum (MECO) and Late Eocene Worming (LEW) events are clearly expressed in our continental record at around ~42–40 Ma ~34.2 Ma, respectively. Overall, our paleoclimatic results suggest that global cooling reduced humidity conditions in the interior of Asia and it may have been responsible for the long-term trend (~52–34) of decreasing chemical weathering in the Xining Basin during the Eocene.

References

Abels H A, Dupont-Nivet G, Xiao G, Bosboom R, Krijgsman W. 2011. Step-wise change of Asian interior climate preceding the Eocene-Oligocene Transition (EOT). Palaeogeogr Palaeoclimatol Palaeoecol, 299: 399–412

Anagnostou E, John E H, Edgar K M, Foster G L, Ridgwell A, Inglis G N, Pancost R D, Lunt D J, Pearson P N. 2016. Changing atmospheric CO_2 concentration was the primary driver of early Cenozoic climate. Nature, 533: 380–384

Bohaty S M, Zachos J C. 2003. Significant Southern Ocean warming event in the late middle Eocene. Geology, 31: 1017–1020

Bosboom R, Dupont-Nivet G, Grothe A, Brinkhuis H, Villa G, Mandic O, Stoica M, Kouwenhoven T, Huang W, Yang W, Guo Z J. 2014. Timing, cause and impact of the late Eocene stepwise sea retreat from the Tarim Basin (west China). Palaeogeogr Palaeoclimatol Palaeoecol, 403: 101–118

Bosboom R E, Dupont-Nivet G, Houben A J P, Brinkhuis H, Villa G, Mandic O, Stoica M, Zachariasse W J, Guo Z J, Li C X, Krijgsman W. 2011. Late Eocene sea retreat from the Tarim Basin (west China) and concomitant Asian paleoenvironmental change. Palaeogeogr Palaeoclimatol Palaeoecol, 299: 385–398

Bracciali L, Najman Y, Parrish R R, Akhter S H, Millar I. 2015. The Brahmaputra tale of tectonics and erosion: Early Miocene river capture in the Eastern Himalaya. Earth Planet Sci Lett, 415: 25–37

Chamley H. 1989. Clay formation through weathering. In: Chamley H, ed. Clay Sedimentology. Berlin: Springer-Verlag. 21–50

CIE. 1978. Recommendations on Uniform Color Spaces, Color-Difference Equations and Psyhometric Color Terms. Paris: Bureau Central de la CIE

Cullers R L. 2000. The geochemistry of shales, siltstones and sandstones of Pennsylvanian-Permian age, Colorado, USA: Implications for provenance and metamorphic studies. Lithos, 51: 181–203

Dabard M P. 1990. Lower Brioverian formations (Upper Proterozoic) of the Armorican Massif (France): Geodynamic evolution of source areas revealed by sandstone petrography and geochemistry. Sediment Geol, 69: 45–58

Dai S, Fang X, Dupont-Nivet G, Song C, Gao J, Krijgsman W, Langereis C, Zhang W. 2006. Magnetostratigraphy of Cenozoic sediments from the Xining Basin: Tectonic implications for the northeastern Tibetan Plateau. J Geophys Res, 111: B11102

Dercourt J, Ricou L E, Vrielinck B. 1993. Atlas Tethys Palaeoenvironmental Maps. Paris: Gauthier-Villars. 307

Dupont-Nivet G, Hoorn C, Konert M. 2008. Tibetan uplift prior to the Eocene-Oligocene climate transition: Evidence from pollen analysis of the Xining Basin. Geology, 36: 987

Dupont-Nivet G, Horton B K, Butler R F, Wang J, Zhou J, Waanders G L. 2004. Paleogene clockwise tectonic rotation of the Xining-Lanzhou region, northeastern Tibetan Plateau. J Geophys Res, 109: B04401

Dupont-Nivet G, Krijgsman W, Langereis C G, Abels H A, Dai S, Fang X. 2007. Tibetan plateau aridification linked to global cooling at the Eocene-Oligocene transition. Nature, 445: 635–638

Duvall A R, Clark M K, van der Pluijm B A, Li C. 2011. Direct dating of Eocene reverse faulting in northeastern Tibet using Ar-dating of fault clays and low-temperature thermochronometry. Earth Planet Sci Lett,

304: 520–526

Fang X, Zan J, Appel E, Lu Y, Song C, Dai S, Tuo S. 2015. An Eocene-Miocene continuous rock magnetic record from the sediments in the Xining Basin, NW China: Indication for Cenozoic persistent drying driven by global cooling and Tibetan Plateau uplift. Geophys J Int, 201: 78–89

Ferrell R E, Brooks R A. 1971. The selective adsorption of sodium by clay minerals in lakes Pontchartrain and Maurepas, Louisiana. Clays Clay Miner, 19: 75–81

Gao X, Hao Q, Wang L, Oldfield F, Bloemendal J, Deng C, Song Y, Ge J, Wu H, Xu B, Li F, Han L, Fu Y, Guo Z. 2018. The different climatic response of pedogenic hematite and ferrimagnetic minerals: Evidence from particle-sized modern soils over the Chinese Loess Plateau. Quat Sci Rev, 179: 69–86

Guo Z T, Berger A, Yin Q Z, Qin L. 2009. Strong asymmetry of hemispheric climates during MIS-13 inferred from correlating China loess and Antarctica ice records. Clim Past, 5: 21–31

Guo Z, Liu T, Fedoroff N, Wei L, Ding Z, Wu N, Lu H, Jiang W, An Z. 1998. Climate extremes in Loess of China coupled with the strength of deep-water formation in the North Atlantic. Glob Planet Change, 18: 113–128

Guo Z T, Ruddiman W F, Hao Q Z, Wu H B, Qiao Y S, Zhu R X, Peng S Z, Wei J J, Yuan B Y, Liu T S. 2002. Onset of Asian desertification by 22 Myr ago inferred from loess deposits in China. Nature, 416: 159–163

Guo Z T, Sun B, Zhang Z S, Peng S Z, Xiao G Q, Ge J Y, Hao Q Z, Qiao Y S, Liang M Y, Liu J F, Yin Q Z, Wei J J. 2008. A major reorganization of Asian climate by the early Miocene. Clim Past, 4: 153–174

Hong H, Wang C, Xu Y, Zhang K, Yin K. 2010. Paleoclimate evolution of the Qinghai-Tibet Plateau since the Cenozoic. Earth Sci-J China Univ of Geosci, 35: 728–736

Hoorn C, Straathof J, Abels H A, Xu Y, Utescher T, Dupont-Nivet G. 2012. A late Eocene palynological record of climate change and Tibetan Plateau uplift (Xining Basin, China). Palaeogeogr Palaeoclimatol Palaeoecol, 344-345: 16–38

Horton B, Dupont-Nivet G, Zhou J, Waanders G, Butler R F, Wang J. 2004. Mesozoic-Cenozoic evolution of the Xining-Minhe and Dangchang basins northeastern Tibetan Plateau: Magnetostratigraphic and biostratigraphic results. J Geophys Res-Solid Earth, 109

Lear C H, Elderfield H, Wilson P A. 2000. Cenozoic deep-sea temperatures and global ice volumes from Mg/Ca in benthic foraminiferal calcite. Science, 287: 269–272

Li C K, Qiu Z D. 1980. Early Miocene mammalian fossils of the Xining Basin Qinghai Province. Vertebrata Palasiatica, 18: 198–209

Licht A, van Cappelle M, Abels H A, Ladant J B, Trabucho-Alexandre J, France-Lanord C, Donnadieu Y, Vandenberghe J, Rigaudier T, Lécuyer C, Terry Jr D, Adriaens R, Boura A, Guo Z, Soe A N, Quade J, Dupont-Nivet G, Jaeger J J. 2014. Asian monsoons in a late Eocene greenhouse world. Nature, 513: 501–506

Liu D, Abuduwaili J, Lei J, Wu G, Gui D. 2011. Wind erosion of saline playa sediments and its ecological effects in Ebinur Lake, Xinjiang, China. Environ Earth Sci, 63: 241–250

Lo F L, Chen H F, Fang J N. 2017. Discussion of suitable chemical weathering proxies in sediments by comparing the dissolution rates of minerals in different rocks. J Geol, 125: 83–99

Long L Q, Fang X M, Miao Y F, Bai Y, Wang Y L. 2011. Northern Tibetan Plateau cooling and aridification linked to Cenozoic global cooling: Evidence from *n*-alkane distributions of Paleogene sedimentary sequences in the Xining Basin. Chin Sci Bull, 56: 1569–1578

Lu J, Song B, Chen R, Zhang J, Ye H. 2010. Palynological assemblage of Eocene-Oligocene pollen and their biostratigraphic correlation in Dahonggou Daqaidam Regions Qaidam Basin. Earth Sci-J Chin Univ Geosci, 35: 839–848

Maher B A. 1998. Magnetic properties of modern soils and Quaternary loessic paleosols: Paleoclimatic implications. Palaeogeogr Palaeoclimatol Palaeoecol, 137: 25–54

Methner K, Mulch A, Fiebig J, Wacker U, Gerdes A, Graham S A, Chamberlain C P. 2016. Rapid middle eocene temperature change in

western north America. Earth Planet Sci Lett, 450: 132–139

Miller K G, Kominz M A, Browning J V, Wright J D, Mountain G S, Katz M E, Sugarman P J, Cramer B S, Christie-Blick N, Pekar S F. 2005. The Phanerozoic record of global sea-level change. Science, 310: 1293–1298

Mosbrugger V, Utescher T, Dilcher D L. 2005. Cenozoic continental climatic evolution of Central Europe. Proc Natl Acad Sci USA, 102: 14964–14969

Nagao S, Nakashima S. 1992. The factors controlling vertical color variations of North Atlantic Madeira Abyssal Plain sediments. Mar Geol, 109: 83–94

Najman Y, Bickle M, BouDagher-Fadel M, Carter A, Garzanti E, Paul M, Wijbrans J, Willett E, Oliver G, Parrish R, Akhter S H, Allen R, Ando S, Chisty E, Reisberg L, Vezzoli G. 2008. The Paleogene record of Himalayan erosion: Bengal Basin, Bangladesh. Earth Planet Sci Lett, 273: 1–14

Nesbitt H W, Markovics G, Price R C. 1980. Chemical processes affecting alkalis and alkaline earths during continental weathering. Geochim Cosmochim Acta, 44: 1659–1666

Nesbitt H W, Young G M, McLennan S M, Keays R R. 1996. Effects of chemical weathering and sorting on the petrogenesis of siliciclastic sediments, with implications for provenance studies. J Geol, 104: 525–542

Nie J, Song Y, King J W, Fang X, Heil C. 2010. HIRM variations in the Chinese red-clay sequence: Insights into pedogenesis in the dust source area. J Asian Earth Sci, 38: 96–104

Pagani M, Zachos J C, Freeman K H, Tipple B, Bohaty S. 2005. Marked decline in atmospheric carbon dioxide concentrations during the paleogene. Science, 309: 600–603

Pearson P N, Foster G L, Wade B S. 2009. Atmospheric carbon dioxide through the Eocene-Oligocene climate transition. Nature, 461: 1110–1113

QBGMR (Qinghai Bureau of Geology and Mineral Resources). 1985. Geologic Maps of the Duoba Gaodian Tianjiazai and Xining Regions 4 Sheets with Regional Geologic Report (1:50000 Scale) (in Chinese). Beijing: Geologial Publishing House. 199

QBGMR (Qinghai Bureau of Geology and Mineral Resources). 1991. Regional Geology of the Qinghai Province (in Chinese). Beijing: Geologial Publishing House. 662

Qiu Z, Qiu Z. 1995. Chronological sequence and subdivision of Chinese Neogene mammalian faunas. Palaeogeogr Palaeoclimatol Palaeoecol, 116: 41–70

Quan C, Liu Y S C, Utescher T. 2012. Paleogene temperature gradient, seasonal variation and climate evolution of northeast China. Palaeogeogr Palaeoclimatol Palaeoecol, 313-314: 150–161

Raymo M E, Ruddiman W F. 1992. Tectonic forcing of late Cenozoic climate. Nature, 359: 117–122

Rieser A B, Bojar A V, Neubauer F, Genser J, Liu Y, Ge X H, Friedl G. 2009. Monitoring Cenozoic climate evolution of northeastern Tibet: Stable isotope constraints from the western Qaidam Basin, China. Int J Earth Sci-Geol Rundsch, 98: 1063–1075

Singh B P. 2013. Evolution of the Paleogene succession of the western Himalayan foreland basin. Geosci Front, 4: 199–212

Song B, Zhang K, Lu J, Wang C, Xu Y, Greenough J. 2013. The middle Eocene to early Miocene integrated sedimentary record in the Qaidam Basin and its implications for paleoclimate and early Tibetan Plateau uplift. Can J Earth Sci, 50: 183–196

Sun J, Jiang M. 2013. Eocene seawater retreat from the southwest Tarim Basin and implications for early Cenozoic tectonic evolution in the Pamir Plateau. Tectonophysics, 588: 27–38

Tada R, Zheng H, Clift P D. 2016. Evolution and variability of the Asian monsoon and its potential linkage with uplift of the Himalaya and Tibetan Plateau. Prog Earth Planet Sci, 3: 4

Taylor S R, McLennan S M. 1985. The Continental Crust: Its Composition and Evolution. Oxford: Blackwell. 312

Timperley M H, Vigor-Brown R J. 1985. Weathering of pumice in the sediments as a possible source of major ions for the waters of Lake Taupo, New Zealand. Chem Geol, 49: 43–52

Torrent J, Barrón V, Liu Q. 2006. Magnetic enhancement is linked to and precedes hematite formation in aerobic soil. Geophys Res Lett, 33: 1–4

Torrent J, Liu Q S, Barrón V. 2010. Magnetic susceptibility changes in relation to pedogenesis in a Xeralf chronosequence in northwestern Spain. Eur J Soil Sci, 61: 161–173

White A F, Blum A E, Bullen T D, Vivit D V, Schulz M, Fitzpatrick J. 1999. The effect of temperature on experimental and natural chemical weathering rates of granitoid rocks. Geochim Cosmochim Acta, 63: 3277–3291

Wronkiewicz D J, Condie K C. 1990. Geochemistry and mineralogy of sediments from the Ventersdorp and Transvaal Supergroups, South Africa: Cratonic evolution during the early Proterozoic. Geochim Cosmochim Acta, 54: 343–354

Wu Y H, Li S J. 2004. Significance of lake sediments color for short time scale climate variation (in Chinese with English abstract). Adv Earth Sci, 19: 789–792

Xiao G Q, Abels H A, Yao Z Q, Dupont-Nivet G, Hilgen F J. 2010. Asian aridification linked to the first step of the Eocene-Oligocene climate Transition (EOT) in obliquity-dominated terrestrial records (Xining Basin, China). Clim Past, 6: 501–513

Xiao G, Guo Z, Dupont-Nivet G, Lu H, Wu N, Ge J, Hao Q, Peng S, Li F, Abels H A, Zhang K. 2012. Evidence for northeastern Tibetan Plateau uplift between 25 and 20 Ma in the sedimentary archive of the Xining Basin, Northwestern China. Earth Planet Sci Lett, 317-318: 185–195

Yang S L, Ding Z L. 2003. Color reflectance of Chinese loess and its implications for climate gradient changes during the last two glacial-interglacial cycles. Geophys Res Lett, 30: 2058

Zachos J C, Dickens G R, Zeebe R E. 2008. An early Cenozoic perspective on greenhouse warming and carbon-cycle dynamics. Nature, 451: 279–283

Zachos J C, Quinn T M, Salamy K A. 1996. High-resolution (10^4 years) deep-sea foraminiferal stable isotope records of the Eocene-Oligocene climate transition. Paleoceanography, 11: 251–266

Zachos J, Pagani M, Sloan L, Thomas E, Billups K. 2001. Trends, rhythms, and aberrations in global climate 65 Ma to present. Science, 292: 686–693

Zhang C, Guo Z T. 2014. Clay mineral changes across the Eocene-Oligocene transition in the sedimentary sequence at Xining occurred prior to global cooling. Palaeogeogr Palaeoclimatol Palaeoecol, 411: 18–29

Zhang J, Wang Y, Zhang B, Zhang Y. 2016. Tectonics of the Xining Basin in NW China and its implications for the evolution of the NE Qinghai-Tibetan Plateau. Basin Res, 28: 159–182

Zhang Z, Wang H, Guo Z T, Jiang D. 2007. What triggers the transition of palaeoenvironmental patterns in China, the Tibetan Plateau uplift or the Paratethys Sea retreat? Palaeogeogr Palaeoclimatol Palaeoecol, 245: 317–331